Thermal and Light-induced Spin-Transition in a Nanometric Film of a New High-Vacuum Processable Spin Crossover Complex

Matteo Atzori,*[,†] Lorenzo Poggini,[‡] Lorenzo Squillantini,[†] Brunetto Cortigiani,[†] Mathieu Gonidec,[‡] Peter Bencok,[‖] Roberta Sessoli,[†] and Matteo Mannini.*[,†]

[†] Dipartimento di Chimica "Ugo Schiff" e INSTM, Università degli Studi di Firenze, Via della Lastruccia 3, I-50019 Sesto Fiorentino (Firenze), Italy.

[‡] Institut de Chimie de la Matière Condensée de Bordeaux, UMR 5026, 87, Avenue du Docteur Schweitzer, F-33608 Pessac Cedex, France.

[‖] Diamond Light Source, Didcot OX11 0DE, United Kingdom.

ELECTRONIC SUPPORTING INFORMATION (ESI)

Powder X-ray Crystallography

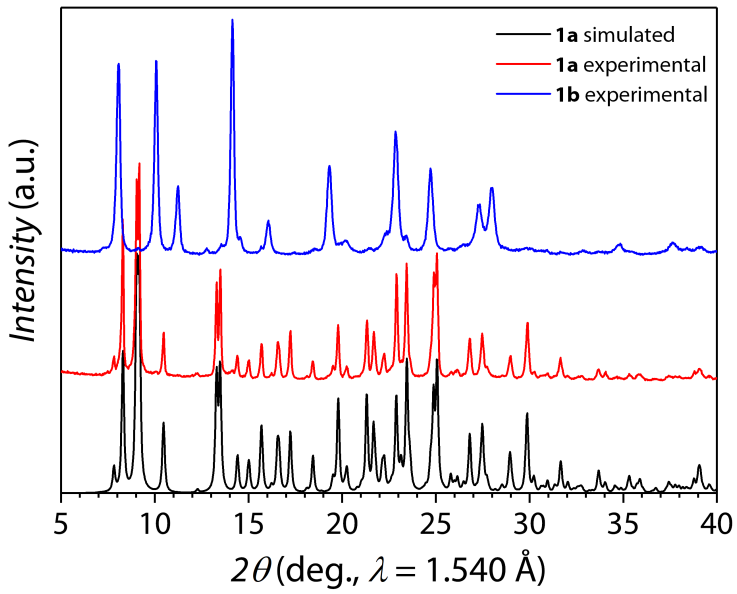

Figure S1. Comparison between experimental and simulated PXRD patterns (5–40°, 2θ) of **1a** and **1b**.

Magnetic and Photomagnetic Measurements

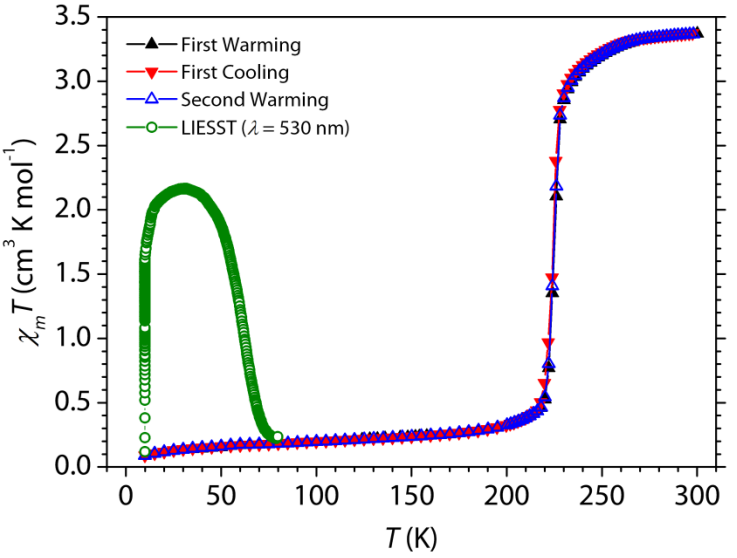

Figure S2. χT versus T plot for **1a** together with photomagnetic measurements associated to the LIESST effect. The χT value is almost zero at low temperature (0–200 K) where only a small residual paramagnetic signal is observed. Above 200 K the χT value abruptly increases reaching the *hs* value of ca. 3.4 cm^3 K mol^{-1} which is in good agreement with the expected value for an Fe^{II} ion with S = 2 and g = 2.1. At 10 K (photoexcitation temperature) the χT value increases, then it reaches a maximum and starts to decrease as the temperature increases. The T_{LIESST} is ca. 60 K.

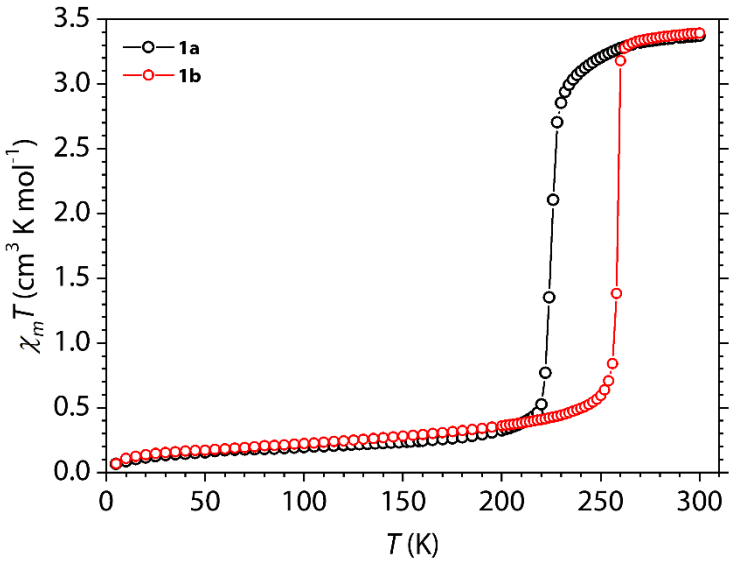

Figure S3. Comparison between the χT versus T plots of **1a** and **1b**.

Thermogravimetric analysis

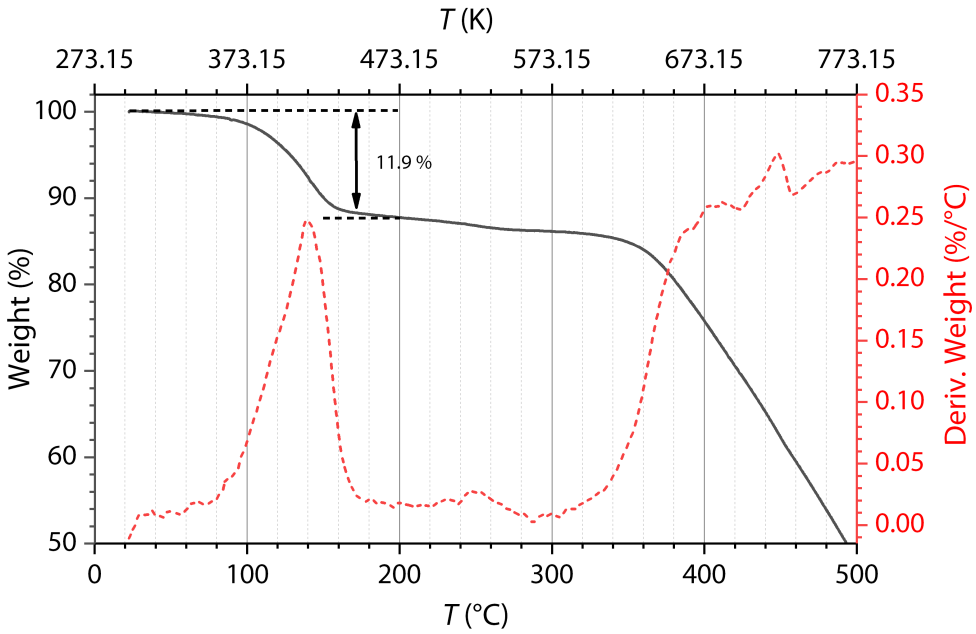

Figure S4. Thermogravimetric analysis data (22–500 °C, scan rate 10 °C/min) for a freshly prepared sample of **1a** (2.090 mg). A weight loss of 11.9 % is clearly observed between ca. 90 and 190 °C corresponding to desolvatation of CH_2Cl_2 crystallization molecules, then the systems remains stable up to ca. 340 °C and if the temperature is increased further it starts to decompose.

Atomic Force Microscopy

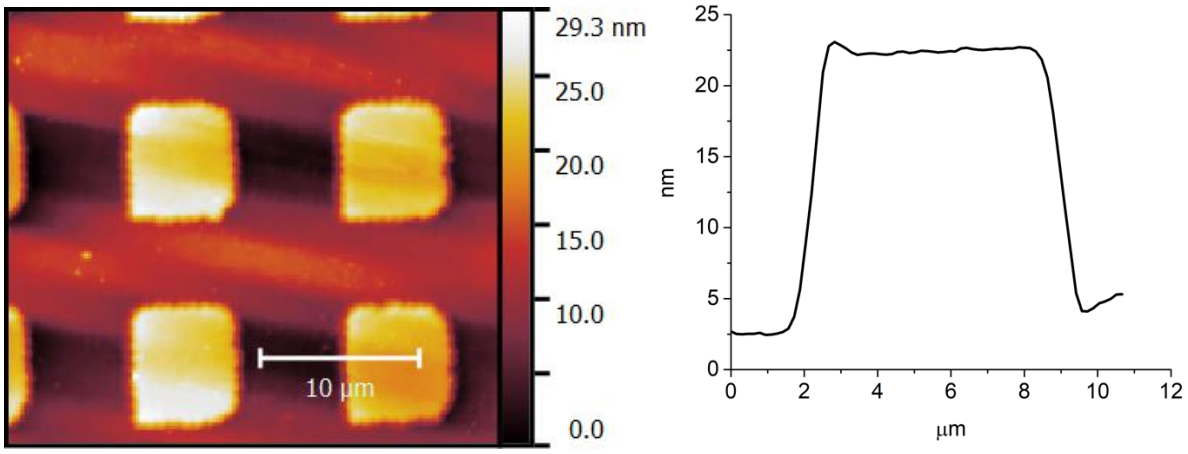

Figure S5. Atomic force microscopy image (left) recorded in tapping mode in air of the patterned deposit of **1** used to calibrate the surface deposition rate during sublimation. This deposit is obtained using the shadow masking method using a transmission electron microscopy grid. In accordance with the vertical profile (right), the estimated thickness of the calibration sample obtained in 2 h was found to be ca. 20(5) nm thus indicating that the adopted conditions lead to a rate of 11(2) nm/h that has been used to produce sample **1c**.

X-ray Crystallography on Thin Films

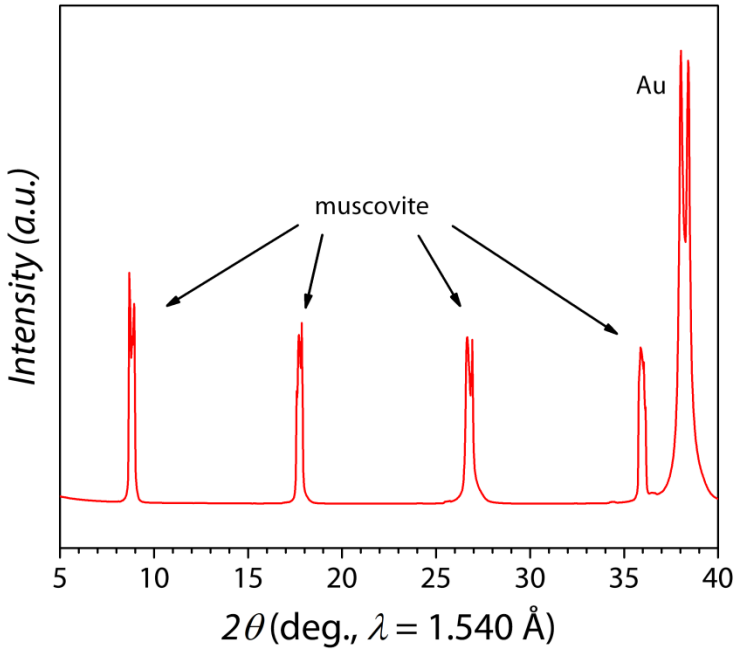

Figure S6. Experimental Wide Angle XRD pattern (5–40°, 2θ) for **1c** in Bragg-Brentano geometry. Only peaks associated to the muscovite and gold are visible.

X-ray Photoelectron Spectroscopy

Table S1. Spectral components used for least squares fitting of the Fe*2p* XPS Binding Energies (*B.E.*). Integrated areas are reported in percentages for each component. Spin-orbit splitting values (ΔE_{SO}) are reported in brackets.

Components	***Fe***$_{A+A'}$, *%;* *B.E.* (ΔE_{SO})	***Fe***$_{B+B'}$, *%;* *B.E.* (ΔE_{SO})	***Fe***$_{C+C'}$, *%;* *B.E.* (ΔE_{SO})	***Fe***$_{D+D'}$, *%;* *B.E.* (ΔE_{SO})
***bulk* (1a)**	45%; 708.5 eV (13.3)	24%; 710.4eV (13.3)	18%; 713.2 eV (13.3)	14%; 716.0 eV (13.3)
***film* (1c)**	42%; 708.5 eV (13.3)	25%; 710.5 eV (13.3)	15%; 713.0 eV (13.3)	18%; 715.8 eV (13.3)

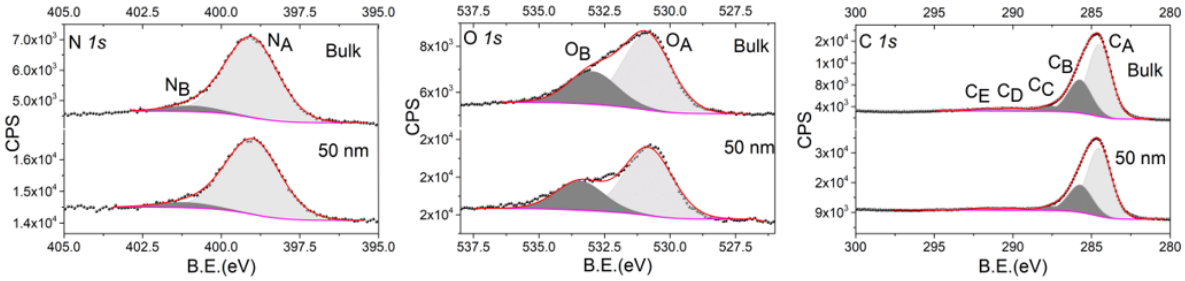

Figure S7. XPS spectra in the N*1s*, O*1s* and C*1s* regions of interest. Black circles indicate the experimental data and red line the resulting fit obtained from the sum of the different components.

X-ray Absorption Spectroscopy

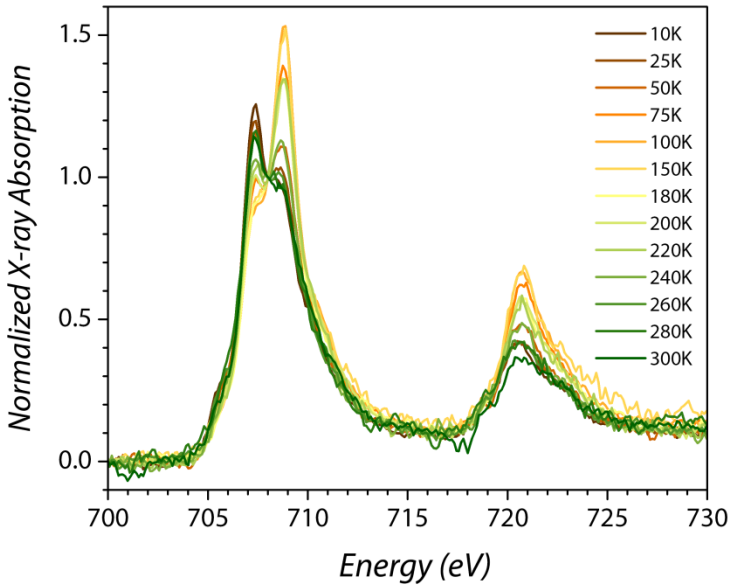

Figure S8. Temperature dependence of the normalized X-ray absorption spectra (700-730 eV) for **1a**.

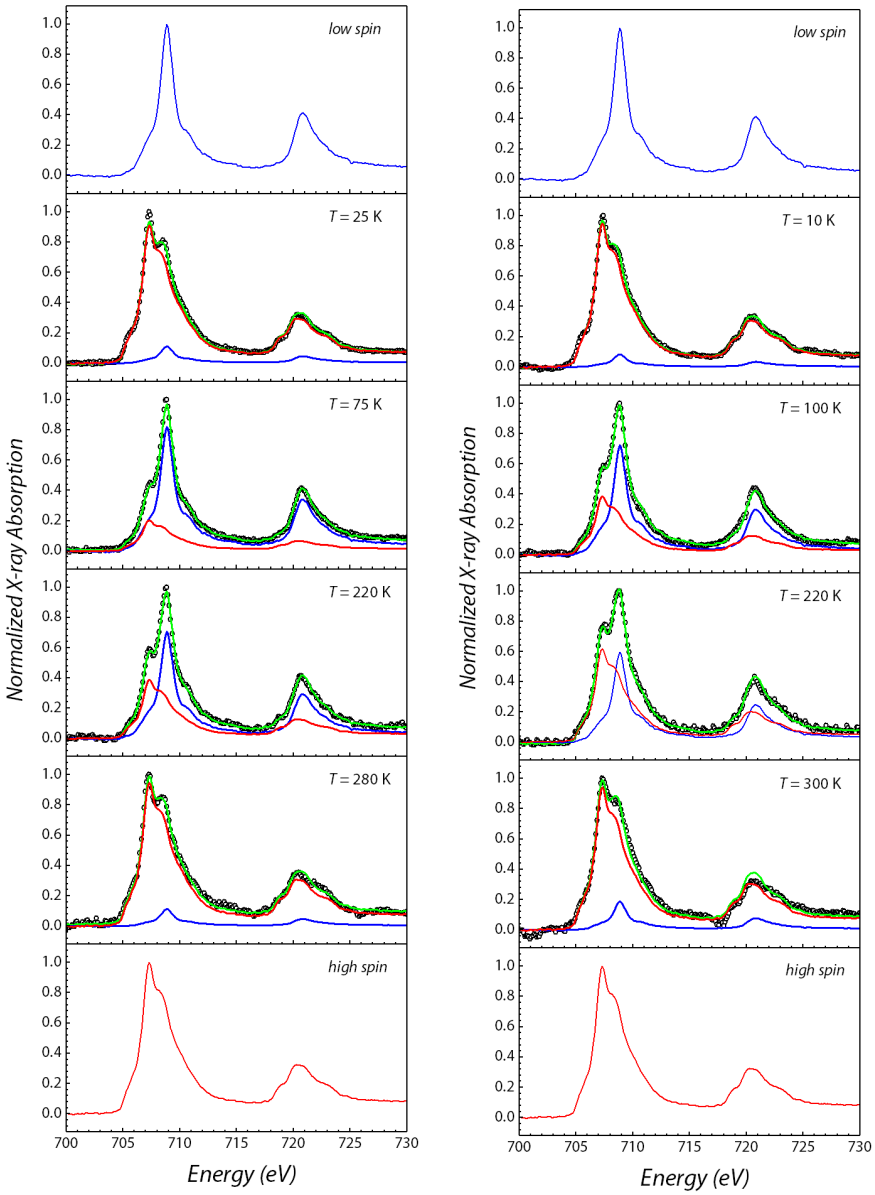

Figure S9. Detail of the experimental XAS spectra (700–730 eV) regression as weighted sum fit of *hs* and *ls* components for **1c** (left) and **1a** (right) at some selected temperatures. Black empty circles are the experimental data, the green line is the best-fit curve, red and blue lines are the *hs* and *ls* contributions, respectively. 100% *hs* (down) and 100% *ls* (top) components are also reported for comparison.

Experimental Section

General remarks. Hqnal (quinoline-naphtaldehyde) and $[Fe(qnal)_2]\cdot CH_2Cl_2$ were synthesized according to the literature procedures.[S1,S2] All other reagents were purchased and used as received. All manipulations were performed under a N_2 inert atmosphere to avoid oxidation of the iron(II) salt before complexation.

Synthesis of $[Fe(qnal)_2]\cdot CH_2Cl_2$ (1a). To a degassed CH_2Cl_2 solution (30 mL) of Hqnal (0.150 g, 0.5 mmol) was added a degassed MeOH solution (20 mL) of $FeSO_4\cdot 7H_2O$ (0.083 mg, 0.3 mmol). A CH_2Cl_2

solution (5 mL) of NEt_3 (0.5 mmol) was added drop-wise to the olive-green solution of the metal complex. This induces an immediate precipitation of a brown microcrystalline solid of **1a**. The suspension was kept under stirring at room temperature for ca. 30 minutes, then the precipitate was filtered, washed with CH_2Cl_2 and then with Et_2O, to provide 0.137 mg of **1a**. Yield 85%. Elemental anal. found (calculated) for $C_{41}H_{28}Cl_2FeN_4O_2$: C% 66.53 (66.96), H% 3.67 (3.84), N% 7.48 (7.62). FT-IR spectroscopy (cm^{-1}, KBr pellet): 3043vw, 1612m, 1565w, 1529s, 1498w, 1455vw, 1422w, 1383s, 1377vs, 1364s, 1299vw, 1194w, 1159vw, 1067vw, 1038vw, 971vw, 823m, 786vw, 753w, 669vw, 567vw, 419vw.

Samples preparation. 1c was obtained by thermal sublimation of **1a** (T = 490 K, deposition rate = 11 nm/s, time = 5 h) on a muscovite surface coated with 20 nm gold. The substrate was prepared using a home-built quartz Knudsen cell in a high vacuum chamber (10^{-7} mbar) at a fixed temperature of 490 K. Thickness of **1c** was estimated controlling the deposition rate through a quartz crystal microbalance. The bulk reference sample used for XPS experiments was prepared scratching a microcrystalline powder of **1a** on an aluminium foil. The bulk reference sample used for XAS experiments was prepared scratching a microcrystalline powder of **1a** on a copper foil.

Characterization. C, H, N analyses were performed with a *CHN-S Flash E1112 Thermofinnigan* analyzer. FT-IR spectra were performed on KBr pellets and collected with a *Shimadzu-8400S* spectrophotometer. Thermogravimetric analysis was performed with a *SDT Q600 TA Instruments (Philadelphia, USA)* analyser.

X-ray Photoelectron Spectroscopy. XPS spectra were carried out in an ultra-high-vacuum (UHV) chamber (10^{-10} mbar range) equipped with VSW hemispherical analyser mounting a 16-channel detector. The X-ray source was a non-monochromatised Al K_α 1486.7 eV (operating at 10 mA, 12 kV, 120 W). The X-ray source was mounted at 54.44° with respect to the analyser. All spectra were measured at normal emission with a fixed pass energy of 44 eV. All the spectra were calibrated to the C*1s* peak at 284.5 eV. Data analysis was performed through the *CasaXPS* software package (1999-2010 CasaXPS Version 2.3.16 casa software Ltd.) using Voigt (30 % lorentzian, 70 % gaussian) curve for all the components, subtracting a linear combination of Shirley and linear baselines (called offset Shirley, 50% Shirley and 50% linear) for Fe*2p* background and a Shirley background for the other elements. Elemental composition of the samples was then evaluated using a semiquantitative analysis: integrated intensity of each component was corrected with the photoionization cross-section[S3] for each atom neglecting the differences in photoelectron escape length as a function of the kinetic energy.

Powder and Thin Films X-ray Crystallography. Wide-Angle Powder X-Ray Diffraction (PXRD) patterns on polycrystalline samples were recorded on a *Bruker New D8 Advance DAVINCI* diffractometer in a theta-theta configuration equipped with a linear detector. The scans were collected

within the range 5–40° (2θ) using CuK_α radiation (λ = 1.540 Å). Simulated patterns were generated from the atomic coordinates of the single-crystal structure solutions using the Mercury CSD 3.5 software[S4] (copyright CCDC, http://www.ccdc.cam.ac.uk/mercury/) using a FWHM (full width at half maximum) of 0.10 and a 2θ step of 0.025. Grazing-Incident X-Ray Diffraction (GIXRD) patterns were recorded on **1c** with a *Bruker New D8 Advance DAVINCI* diffractometer with a linearly focalized X-ray beam through a focusing mirror. The incident angle has been varied in the 0.2–10° range, and the scans were collected within the 2θ range 5–40°, using CuK_α radiation (λ = 1.540 Å).

Magnetic Measurements. Susceptibility measurements were performed in the 2.0–300 K temperature range with an applied magnetic field of 1.0 T on polycrystalline samples of compounds **1a** and **1b** with masses of 8.00 mg and 9.10 mg, respectively, by using a *Quantum Design MPMS-XL-5 SQUID* magnetometer. Photomagnetic measurements were performed on a KBr pellet of **1a** containing ca. 0.5 mg microcrystalline powder. The effective mass of the paramagnetic component was evaluated by scaling the resulting magnetic susceptibility obtained before irradiation experiments with respect to the contribution provided by the pure compound previously measured under the same conditions (*vide supra*). Irradiation experiments have been performed by using a 530 nm wavelength continuous wave laser diode with an optical fiber inserted in the sample space through a hollow sample rod and collimated on the sample by means of an aspheric lens. The radiant power on the sample was ca. 5 mW cm^{-2}. The excitation wavelength was selected on the basis of previously performed photomagnetic measurements on the same compound and its UV-Vis absorption spectrum.[2] T_{LIESST} measurement were performed after 2 hours irradiation of the sample at 10 K, by measuring the magnetic susceptibility on increasing the temperature at a rate of 0.3 K/min after having switched off the laser. Susceptibility data were corrected for the sample holders previously measured using the same conditions and for the diamagnetic contributions as deduced by using Pascal's constant tables.[S5]

Atomic Force Microscopy. Morphological analysis has been carried out with a NT-MDT Solver P47pro Scanning Probe Microscope (NT-MDT, Zelenograd, Moscow, Russia; www.ntmdt.ru). AFM images were recorded in tapping mode in air using a NSC36B n-type silicon tip (MikroMash) with a resonance frequency of 150 KHz.

X-ray Absorption Spectroscopy. The XAS experiments were performed on **1a** and **1c**. The photon flux was reduced to prevent any radiation damage. No degradation during the experiments was observed. A magnetic field up to 30 kOe was applied along the photon propagation direction at variable angle with the normal to the surface. The reported XAS spectra were acquired at the $L_{2,3}$ edges of Fe (applied parallel to the X-ray propagation vector) and using the two circular polarizations (left, σ+ and right, σ-) at normal incidence (θ = 0°). All spectra were normalized following the procedures described in earlier reports.[S6] Absorption spectra were measured in Total Electron Yield (TEY) detection mode to guarantee

the optimal detection sensitivity. The temperature dependence of the *hs*-Fe(II) molar fraction of **1a** and **1c** was qualitatively estimated through least-squares interpolation of the normalized XAS spectra by using two reference spectra of the bulk compound recorded at 300 K and 100 K, for *hs* and *ls* contributions respectively, to exclude the SOXIEEST effect.[S7]

The light irradiation was carried out irradiating the sample from outside through an optical viewport at the base temperature of 10 K using a Thorlabs CLD1010LP controlled equipped with a 520 nm laser diode (520-SF15), an optical fibre and a collimator to focus the light on the sample. The optical output power on the laser controller was fixed at 10 mW while the diode temperature controller was stabilized to 25 ± 0.1 °C. No increase of sample temperature was detected during the irradiation period.

Supplementary References

S1. Tisato, F.; Refosco, F.; Moresco, A.; Bandoli, G.; Mazzi, U.; Nicolini, M. *J. Chem. Soc., Dalton Trans.*, **1990**, 2225.

S2. Kuroda-Sowa, T.; Yu, Z; Senzaki, Y.; Sugimoto, K.; Maekawa, M.; Munakata, M.; Hayami, S.; Maeda, Y. *Chem. Lett.* **2008**, *37*, 1216.

S3. (a) http://ulisse.elettra.trieste.it. (b) Yeh, J. J.; Lindau, I. *Atomic Data and Nuclear Data Tables* **1985**, *32*, 1–155.

S4. Macrae, C. F.; Edgington, P. R.; McCabe, P.; Pidcock, E.; Shields, G. P.; Taylor, R.; Towler, M.; van de Streek, J. Mercury: visualization and analysis of crystal structures. *J. Appl. Crystallogr.* **2006**, *39*, 453.

S5. Bain, G. A.; Berry, J. F. *J. Chem. Educ.* **2008**, *85*, 532.

S6. Margheriti, L.; Chiappe, D.; Mannini, M.; Car, P.-E.; Sainctavit, P.; Arrio, M.-A.; de Mongeot, F. B.; Cezar, J. C.; Piras, F. M.; Magnani, A. Otero, E.; Caneschi, A.; Sessoli, R. *Adv. Mater.* **2010**, *22*, 5488.

S7. Warner, B.; Oberg, J. C.; Gill, T. G.; El Hallak, F.; Hirjibehedin, C. F.; Serri, M.; Heutz, S.; Arrio, M.-A.; Sainctavit, P.; Mannini, M.; Poneti, G.; Sessoli, R.; Rosa, P. *J. Phys. Chem. Lett.* **2013**, *4*, 1546.